Linear and nonlinear excitations in two stacks of parallel arrays of long Josephson junctions

Carapella, G.; Constabile, Giovanni; Latempa, R.; Filatrella, G.; Mygind, Jesper

Published in:
Physical Review B (Condensed Matter and Materials Physics)

Link to article, DOI:
10.1103/PhysRevB.62.9095

Publication date:
2000

Document Version
Publisher's PDF, also known as Version of record

Linear and nonlinear excitations in two stacks of parallel arrays of long Josephson junctions

G. Carapella, G. Costabile, R. Latempa, and G. Filatrella
Unità INFM and Dipartimento di Fisica, Università di Salerno, I-84081 Baronissi, Italy

J. Mygind
Department of Physics, B309, The Technical University of Denmark, DK-2800 Lyngby, Denmark
(Received 16 December 1999; revised manuscript received 22 March 2000)

We investigate a structure consisting of two parallel arrays of long Josephson junctions sharing a common electrode that allows inductive coupling between the arrays. A model for this structure is derived starting from the description of its continuous limit. The excitation of linear cavity modes known from continuous and discrete systems as well as the excitation of a new state exhibiting synchronization in two dimensions are inferred from the mathematical model of the system. The stable nonlinear solution of the coupled sine-Gordon equations describing the system is found to consist of a fluxon-antifluxon string. This is a two-dimensional phase-locked solitonic mode. Both linear and nonlinear excitations are numerically investigated and experimentally demonstrated in two stacks of five-junction arrays.

I. INTRODUCTION

Long Josephson junctions are very attractive systems where linear as well as nonlinear excitations are fully developed and directly related to experimentally observable quantities. Linear (or quasilinear) excitations principally consist of cavity modes along the length of the junction[1,2] excited by means of the current oscillations associated to the ac Josephson effect, while the typical nonlinear excitation is a solitonic solution of the sine-Gordon equation[3] describing the long junction and is physically represented by a fluxon, a current vortex enclosing a flux quantum. These two kind of excitations correspond to distinct current singularities in the current-voltage characteristic of the junction. Moreover, when we bias the junctions on these singularities, an ac signal in the microwave range is received. This is why the Josephson junctions are also known as Josephson oscillators[4] and deserve an interest in microwave electronics. Coherent excitations in coupled structures of Josephson junctions, as synchronized linear modes or phase-locked fluxon modes are an intriguing physical subject, where linear as well as nonlinear dynamics play a comparable role. The analysis of coupled structures demonstrating stable coherent states can deserve some interest also because of possible practical applications. In fact, microwave and far infrared oscillators[4] greatly enhance their performance if such excitations are established. For this purpose, stacks of magnetically coupled long Josephson junctions were proved to be good candidates. It was shown theoretically[5–8] and experimentally that linear[9–11] and nonlinear[12,13] excitations can be synchronized in these systems. Moreover, also arrays made of short,[14–17] and long[18–20] Josephson junctions have been experimentally demonstrated capable of mutual synchronization.

In this paper we propose and study an hybrid structure, consisting of a two stack of magnetically coupled parallel arrays of long Josephson junctions. This structure is, in our opinion, an interesting physical example where coupling of discrete and continuous dynamical systems can be recovered. For example, in some regime the system is described by Frenkel-Kontorova chains coupled by both continuous and discrete terms. Also, due to the hybridation between planar and vertical integration, we can expect the structure to be capable to support states where both planar and vertical synchronization are achieved. A synchronization involving more than one dimension obviously enhances the robustness and the stability of the coherent state that is achieved, an important for practical applications. As we will see, the nonlinear coherent state in the structure consist of fluxon-antifluxon pairs arranged in more or less rigid strings, oscillating across the long dimension of the junctions. The linear coherent state consists of cavity modes along the length of the junctions synchronized both in the planar and in the vertical dimensions of the structure.

The paper is organized as follows. In Sec. II we derive the model for the physical system starting from the description of its continuous limit, i.e., a two stack of two-dimensional Josephson junctions. We obtain the dispersion relation for electromagnetic waves in the coupled structure linearizing the coupled sine-Gordon equations that describe the system. We analyze the excitation of cavity mode resonances in the structure providing an approximate analytic form as well as the analytic prediction of the excitation frequencies. Nonlinear waves solutions are then found, and their stability is discussed considering the interaction energy in the nearest-neighbor approximation. Hence an analytic expression is given for the current-voltage (I-V) characteristic representing the stable oscillations of the fluxon-antifluxon string. In Sec. III we further discuss the cavity modes and the fluxon-antifluxon string with the help of numerical simulations and we provide an analysis of the electromagnetic signals expected at one edge of the structure operated in a cavity mode. In Sec. IV we report on the experimental demonstration of excitation of cavity mode resonances and fluxon-antifluxon strings in two stacks of five-junction arrays and we compare their I-V curves with the theoretical predictions. A summary of the main results of the paper is finally given in Sec. V.

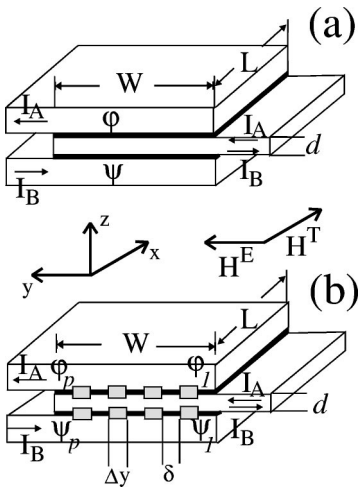

FIG. 1. (a) Sketch of a two-dimensional double overlap stack. (b) Two stack of parallel arrays of p long Josephson junctions.

II. THEORY

To model our two stack of parallel arrays of long Josephson junctions [see Fig. 1(b)], we start from the description of the two-dimensional double overlap stack in Fig. 1(a) which is modelled as[21]

$$\varphi_{xx}+\varphi_{yy}-\varphi_{tt}=\sin\varphi+\alpha\varphi_t+\varepsilon(\psi_{xx}+\psi_{yy}), \tag{1a}$$

$$\psi_{xx}+\psi_{yy}-\psi_{tt}=\sin\psi+\alpha\psi_t+\varepsilon(\varphi_{xx}+\varphi_{yy}), \tag{1b}$$

$$\varphi_x(0)=\varphi_x(l)=(1+\varepsilon)\,\eta^E, \tag{1c}$$

$$\psi_x(0)=\psi_x(l)=(1+\varepsilon)\,\eta^E, \tag{1d}$$

$$\varphi_y(0)=-(1+\varepsilon)\,\eta^T-\frac{w}{(1+\varepsilon)}\,\frac{\gamma_A-\gamma_B}{2}, \tag{1e}$$

$$\varphi_y(w)=-(1+\varepsilon)\,\eta^T+\frac{w}{(1+\varepsilon)}\,\frac{\gamma_A+\gamma_B}{2}, \tag{1f}$$

$$\psi_y(0)=-(1+\varepsilon)\,\eta^T-\frac{w}{(1+\varepsilon)}\,\frac{\gamma_B-\gamma_A}{2}, \tag{1g}$$

$$\psi_y(w)=-(1+\varepsilon)\,\eta^T+\frac{w}{(1+\varepsilon)}\,\frac{\gamma_A+\gamma_B}{2}, \tag{1h}$$

where φ, and ψ are the Josephson phase differences, $-1<\varepsilon<0$ is the magnetic coupling constant, defined as a function of the thickness d of the intermediate electrode, of the thickness t of the insulating barriers, and of the London penetration depth λ_L by[5]

$$\varepsilon=-\frac{\lambda_L}{\sinh(d/\lambda_L)}\,\frac{1}{[t+\lambda_L+\lambda_L\coth(d/\lambda_L)]}. \tag{2}$$

The lengths in Eqs. (1) are normalized to the Josephson penetration length

$$\lambda_J=\sqrt{\frac{\hbar c^2}{8\pi e d'(1-\varepsilon^2)J_0}},$$

where $d'=t+\lambda_L+\lambda_L\coth(d/\lambda_L)$ and J_0 is the critical current density of the junctions. The time is normalized to the inverse of the plasma frequency $\omega_J=\overline{c}/\lambda_J$, where

$$\overline{c}=c\sqrt{\frac{t}{\varepsilon_r d'(1-\varepsilon^2)}}$$

is the Swihart velocity. Furthermore, $l=L/\lambda_J$ is the normalized length and $w=W/\lambda_J$ is the normalized width of the junctions, $\alpha=(1/R)\sqrt{\hbar/2eCJ_0}$ is the Ohmic dissipation, and $\gamma_{A,B}=I_{A,B}/J_0LW$ are the normalized bias currents [see Fig. 1(a)]. Finally, $\eta^{T,E}=H^{T,E}/H_c$ are the components of an externally applied magnetic field $\mathbf{H}\equiv(H^T,H^E,0)$ [see Fig. 1(a)], normalized to the critical field $H_c=(4\pi/c)\lambda_J J_0(1-\varepsilon^2)$.

Assuming the junctions in the parallel arrays as one dimensional [i.e., $\delta\ll\lambda_J$, see Fig. 1(b)], the structure in Fig. 1(b) becomes the continuous system of Fig. 1(a) in the limit

$$p\to\infty,\quad \Delta y\to 0;\quad p\Delta y=W.$$

For a finite separation between the junctions Δy and for a finite number of junctions p, we can think of the system in Fig. 1(b) as the y -discretized version of the continuous system in Fig. 1(a). Thus the model for the two stack of parallel arrays of long Josephson junctions can be obtained by discretizing the model Eqs. (1) in the y direction,

$$\varphi(x,y)\to\varphi[x,(n-1)\sqrt{\beta}]\equiv\varphi_n(x), \tag{3a}$$

$$\psi(x,y)\to\psi[x,(n-1)\sqrt{\beta}]\equiv\psi_n(x), \tag{3b}$$

where we have defined $\beta\equiv(\Delta y/\lambda_J)^2$. Hence our model is

$$\varphi_{ntt}=\varphi_{nxx}-\sin\varphi_n-\alpha\varphi_{nt}-\varepsilon\psi_{nxx}+\frac{1}{\beta}(\varphi_{n+1}-2\varphi_n+\varphi_{n-1})$$
$$-\frac{\varepsilon}{\beta}(\psi_{n+1}-2\psi_n+\psi_{n-1}),\quad 2\leqslant n\leqslant p-1, \tag{4a}$$

$$\psi_{ntt}=\psi_{nxx}-\sin\psi_n-\alpha\psi_{nt}-\varepsilon\varphi_{nxx}+\frac{1}{\beta}(\psi_{n+1}-2\psi_n+\psi_{n-1})$$
$$-\frac{\varepsilon}{\beta}(\varphi_{n+1}-2\varphi_n+\varphi_{n-1}),\quad 2\leqslant n\leqslant p-1, \tag{4b}$$

$$\varphi_{1tt}=\varphi_{1xx}-\sin\varphi_1-\alpha\varphi_{1t}-\varepsilon\psi_{1xx}+\frac{2}{\beta}(\varphi_2-\varphi_1)$$
$$-\frac{2\varepsilon}{\beta}(\psi_2-\psi_1)+\frac{2}{\sqrt{\beta}}(1-\varepsilon^2)\,\eta^T+(p-1)(\gamma_A-\gamma_B), \tag{4c}$$

$$\psi_{1tt}=\psi_{1xx}-\sin\psi_1-\alpha\psi_{1t}-\varepsilon\varphi_{1xx}+\frac{2}{\beta}(\psi_2-\psi_1)$$
$$-\frac{2\varepsilon}{\beta}(\varphi_2-\varphi_1)+\frac{2}{\sqrt{\beta}}(1-\varepsilon^2)\,\eta^T+(p-1)(\gamma_B-\gamma_A), \tag{4d}$$

$$\varphi_{ptt}=\varphi_{pxx}-\sin\varphi_p-\alpha\varphi_{pt}-\varepsilon\psi_{pxx}+\frac{2}{\beta}(\varphi_{p-1}-\varphi_p)$$
$$-\frac{2\varepsilon}{\beta}(\psi_{p-1}-\psi_p)-\frac{2}{\sqrt{\beta}}(1-\varepsilon^2)\eta^T$$
$$+(p-1)(\gamma_A+\gamma_B), \tag{4e}$$

$$\psi_{ptt}=\psi_{pxx}-\sin\psi_p-\alpha\psi_{pt}-\varepsilon\varphi_{pxx}+\frac{2}{\beta}(\psi_{p-1}-\psi_p)$$
$$-\frac{2\varepsilon}{\beta}(\varphi_{p-1}-\varphi_p)-\frac{2}{\sqrt{\beta}}(1-\varepsilon^2)\eta^T$$
$$+(p-1)(\gamma_A+\gamma_B), \tag{4f}$$

$$\varphi_{nx}(0)=\varphi_{nx}(l)=(1+\varepsilon)\eta^E, \quad 1\leqslant n\leqslant p, \tag{4g}$$

$$\psi_{nx}(0)=\psi_{nx}(l)=(1+\varepsilon)\eta^E. \quad 1\leqslant n\leqslant p \tag{4h}$$

A. Linear excitations

In the absence of perturbations and in the nontunneling limit [i.e., $\gamma_A=\gamma_B=\eta^T=\eta^E=\alpha=\sin\varphi_n=\sin\psi_n=0$], the structure in Fig. 1(b) becomes a system of coupled transmission lines. If, for the sake of simplicity, we neglect the edge lines ($n=1$, and $n=p$), the system is described by

$$\varphi_{nxx}-\varepsilon\psi_{nxx}+\frac{1}{\beta}(\varphi_{n+1}-2\varphi_n+\varphi_{n-1})$$
$$-\frac{\varepsilon}{\beta}(\psi_{n+1}-2\psi_n+\psi_{n-1})-\varphi_{ntt}=0, \tag{5a}$$

$$\psi_{nxx}-\varepsilon\varphi_{nxx}+\frac{1}{\beta}(\psi_{n+1}-2\psi_n+\psi_{n-1})$$
$$-\frac{\varepsilon}{\beta}(\varphi_{n+1}-2\varphi_n+\varphi_{n-1})-\psi_{ntt}=0. \tag{5b}$$

The dispersion relation for linear electromagnetic waves in the structure is obtained by substituting a plane-wave solution

$$\varphi_n(x)=Ae^{i[k_x x+(n-1)\sqrt{\beta}k_y-\omega t]}, \tag{6a}$$

$$\psi_n(x)=Be^{i[k_x x+(n-1)\sqrt{\beta}k_y-\omega t]}, \tag{6b}$$

in Eqs. (5). The result is

$$\omega^{\pm}=u^{\pm}\sqrt{k_x^2+\frac{4}{\beta}\sin^2\frac{k_y\sqrt{\beta}}{2}}, \tag{7}$$

where $u^+=\sqrt{1+|\varepsilon|}$ is the characteristic velocity corresponding to the in-phase ($A=B$) mode, and $u^-=\sqrt{1-|\varepsilon|}$ is the velocity corresponding to the out-of-phase ($A=-B$) mode in the structure.

Cavity mode resonances are found looking for solutions that satisfy open circuit boundary conditions (B.C.'s). In the continuous system of Fig. 1(a) the B.C.'s are

$$\varphi_x(0)=\varphi_x(l)=\psi_x(0)=\psi_x(l)=0,$$
$$\varphi_y(0)=\varphi_y(w)=\psi_y(0)=\psi_y(w)=0,$$

and spatial cavity modes have the form $\varphi=\pm\psi\propto\cos k_x x\cos k_y y$ with wave numbers $k_x=j\pi/l$, $k_y=m\pi/w$ (j,m integers). In the y-discretized system of Fig. 1(b), the k_y is simply found noticing that here $w=(p-1)\sqrt{\beta}$, while k_x is the same as in the continuous system. Hence the cavity mode resonances in the two stack of parallel arrays will have wave numbers

$$k_x=\frac{j\pi}{l}, \quad j=1,2\ldots, \tag{8a}$$

$$k_y=\frac{m\pi}{(p-1)\sqrt{\beta}} \quad m=1,2\ldots \tag{8b}$$

and hence, from relation (7), frequencies

$$\omega_{j,m}^{\pm}=u^{\pm}\sqrt{\left(\frac{j\pi}{l}\right)^2+\frac{4}{\beta}\sin^2\frac{m\pi}{2(p-1)}}. \tag{9}$$

Therefore in our system the dispersion relation exhibited by a parallel array of long Josephson junctions[19] splits in two branches.

The resonances described by Eq. (9) are practically excited by a magnetic field and appear as current singularities in the I-V characteristic. If we apply only a magnetic field along the y direction, we have $k_y=0$. From Eqs. (8) and (9) the cavity modes (Fiske steps) will have excitation frequencies

$$\omega_{j,0}^{\pm}=u^{\pm}\left(\frac{j\pi}{l}\right)=j\Delta V_{FS}^{\pm}. \tag{10}$$

The functional form of these cavity modes (eigenvectors associated to frequencies $\omega_{j,0}^{\pm}$) can be inferred from the ansatz Eqs. (6) and (8a) as

$$\psi_n^{(ac)}=\pm\varphi_n^{(ac)}\sim A(\omega)\cos\left(\frac{j\pi}{l}x\right)\cos(\omega t) \quad 1\leqslant n\leqslant p, \tag{11}$$

where $A(\omega)$ will be maximum when the resonance condition $\omega=\omega_{j,0}^{\pm}$ is satisfied, and where we used the notation $\varphi_n^{(ac)}$, $\psi_n^{(ac)}$ to indicate the oscillating component of the phases that account for the excitation of a cavity mode.

If we apply a magnetic field in the x direction, we have $k_x=0$. From Eqs. (8) and (9) the cavity modes will have now excitation frequencies

$$\omega_{0,m}^{\pm}=u^{\pm}\frac{2}{\sqrt{\beta}}\left|\sin\frac{m\pi}{2(p-1)}\right|, \tag{12}$$

with associated eigenvectors of the form

$$\psi_n^{(ac)}=\pm\varphi_n^{(ac)}\sim A(\omega)\cos\left[\frac{(n-1)m\pi}{(p-1)}\right]\cos(\omega t), \quad 1\leqslant n\leqslant p, \tag{13}$$

where, again, $A(\omega)$ will be maximum when the resonance condition $\omega=\omega_{0,m}^{\pm}$ is satisfied.

In the experimental *I-V* characteristic of the device, the resonances excited by a magnetic field in the *y* direction will correspond to current singularities with asymptotic voltages

$$V_j^{\pm}=j\Phi_0\overline{c^{\pm}}/2L=j\Phi_0\overline{c}\sqrt{1\pm|\varepsilon|}/2L=j\Delta V_{FS}^{\pm}, \qquad (14)$$

where L is the physical length of the junctions, Φ_0 is the flux quantum and $\overline{c}$ is the Swihart velocity in the stack. In other words we expect two series of singularities, with characteristic voltage spacing $\Delta V_{FS}^{\pm}$ corresponding to the two velocities allowed in the structure. Conversely, the resonances excited by a magnetic field in the *x* direction will appear as two series of singularities not evenly spaced, with asymptotic voltages

$$V_m^{\pm}=\overline{c^{\pm}}\frac{\Phi_0}{\Delta y}\left|\sin\frac{m\pi}{2(p-1)}\right|, \qquad (15)$$

and upper limited by the maximum voltages $V_{\max}^{\pm}=\overline{c^{\pm}}\Phi_0/\Delta y$.

B. Nonlinear excitations

Possibly, many soliton arrangements can be expected in the structure, each one deserving attention for some interesting properties. Here we will focus on the solutions exhibiting 2D synchronization. This subclass of all possible solutions will be necessarily symmetric. A symmetric ansatz is

$$\varphi_n=\phi, \qquad (16a)$$

$$\psi_n=\sigma\phi, \qquad (16b)$$

where $n=1,\ldots,p$, $\sigma=\pm1$, that reduces the unperturbed $[\gamma_A=\gamma_B=\eta^T=\eta^E=\alpha=0]$ coupled sine-Gordon system Eqs. (4a)–(4f) to

$$\phi_{tt}=(1-\sigma\varepsilon)\phi_{xx}-\sin\phi.$$

Assuming infinite-length junctions for the sake of simplicity, the basic solitonic solution of this equation is[23]

$$\phi=4\tan^{-1}\left\{\exp\left[\gamma\left(\frac{u}{\sqrt{1-\sigma\varepsilon}}\right)\frac{x-ut}{\sqrt{1-\sigma\varepsilon}}\right]\right\}, \qquad (17)$$

where $\gamma(z)=1/\sqrt{1-z^2}$, and u is the velocity of the traveling solution. For a given n, Eqs. (16) and (17) describe a fluxon-fluxon pair ($\sigma=+1$), or a fluxon-antifluxon pair ($\sigma=-1$). Hence the two fundamental solitonic solutions of our unperturbed coupled system are a fluxon-fluxon string,

$$\psi_n=\varphi_n=\phi=4\tan^{-1}\left\{\exp\left[\gamma\left(\frac{u}{u^+}\right)\frac{x-ut}{\sqrt{1-\varepsilon}}\right]\right\}, \quad 1\leqslant n\leqslant p, \qquad (18)$$

traveling with asymptotic velocity $u^+=\sqrt{1-\varepsilon}$, or a fluxon-antifluxon string,

$$\psi_n=-\varphi_n=-\phi=-4\tan^{-1}\left\{\exp\left[\gamma\left(\frac{u}{u^-}\right)\frac{x-ut}{\sqrt{1+\varepsilon}}\right]\right\}, \quad 1\leqslant n\leqslant p, \qquad (19)$$

traveling with asymptotic velocity $u^-=\sqrt{1+\varepsilon}$.

We should remark that with ansatz Eqs. (16) we implicitly suppressed the possibility of excitation of solitonic modes along the *y* direction. In fact, such a kind of excitations have been discussed in related works[16,20] on the single barrier version of our structure. In particular, both in unidimensional overlap junctions with regular arrays of defects[16] and in bidimensional[20] overlap junctions with columnar defects it is found that solitonic excitations occur along the discretized dimension when this dimension is quite larger than Josephson penetration length. On this basis, we consider our fluxon-fluxon or fluxon-antifluxon strings as the candidate solitonic solutions of our structure when the discretized dimension is not quite large with respect to the Josephson penetration length.

Information on the stability of these solutions can be obtained from the interaction energy between the solitons constituting the strings. For this we need to set the Hamiltonian of the system.

1. Interaction energy between nearest-neighbors solitons

The unperturbed coupled sine-Gordon system $[\gamma_A=\gamma_B=\eta^T=\eta^E=\alpha=0$ in Eqs. (4)] follows from the Eulero-Lagrange equations if the following Hamiltonian density is chosen

$$\begin{aligned}\overline{H}=&\sum_{m=2}^{p-1}\{\overline{H}_{SG}[\varphi_m]+\overline{H}_{SG}[\psi_m]+\overline{H}_{\varepsilon}[\varphi_m,\psi_m]\}+\frac{1}{2}\overline{H}_{SG}[\varphi_1]\\&+\frac{1}{2}\overline{H}_{SG}[\psi_1]+\frac{1}{2}\overline{H}_{\varepsilon}[\varphi_1,\psi_1]+\frac{1}{2}\overline{H}_{SG}[\varphi_p]+\frac{1}{2}\overline{H}_{SG}[\psi_p]\\&+\frac{1}{2}\overline{H}_{\varepsilon}[\varphi_p,\psi_p]+\sum_{m=2}^{p}\{\overline{H}_{\beta}[\varphi_m,\varphi_{m-1}]+\overline{H}_{\beta}[\psi_m,\psi_{m-1}]\\&+\overline{H}_{\varepsilon\beta}[\varphi_m,\psi_m]\},\end{aligned}$$

where

$$\overline{H}_{SG}[\varphi_m]=\frac{1}{2}\varphi_{mx}^2+\frac{1}{2}\varphi_{mt}^2+1-\cos\varphi_m, \qquad (20a)$$

$$\overline{H}_{\beta}[\varphi_m,\varphi_{m-1}]=\frac{1}{2\beta}(\varphi_m-\varphi_{m-1})^2, \qquad (20b)$$

$$\overline{H}_{\varepsilon}[\varphi_m,\psi_m]=-\varepsilon\varphi_{mx}\psi_{mx}, \qquad (20c)$$

$$\overline{H}_{\varepsilon\beta}[\varphi_m,\psi_m]=-\frac{\varepsilon}{\beta}(\varphi_m-\varphi_{m-1})(\psi_m-\psi_{m-1}). \qquad (20d)$$

As it is seen in Eqs. (20), elastic ($\overline{H}_{\beta}$), magnetic ($\overline{H}_{\varepsilon}$), and discrete-magnetic ($\overline{H}_{\varepsilon\beta}$) interactions coexist in the system.

The total energy of the system is

$$H=\int_{-\infty}^{+\infty}\overline{H}dx, \qquad (21)$$

while the interaction energy between nearest-neighbor soliton pairs is

$$E_I=\int_{-\infty}^{+\infty}\{\overline{H}_\beta[\varphi_m,\varphi_{m-1}]+\overline{H}_\beta[\psi_m,\psi_{m-1}]+\overline{H}_\varepsilon[\psi_m,\varphi_m]+\overline{H}_{\varepsilon\beta}[\varphi_m,\psi_m]\}dx$$
$$=\int_{-\infty}^{+\infty}\left\{\frac{1}{2\beta}(\varphi_m-\varphi_{m-1})^2+\frac{1}{2\beta}(\psi_m-\psi_{m-1})^2\right\}dx+\int_{-\infty}^{+\infty}\left\{-\varepsilon\varphi_{mx}\psi_{mx}-\frac{\varepsilon}{\beta}(\varphi_m-\varphi_{m-1})\times(\psi_m-\psi_{m-1})\right\}dx. \quad (22)$$

A basic set of nearest-neighbors solitons can be described by

$$\varphi_m=4\tan^{-1}\left\{\exp\left[\Lambda\left(x-\frac{\mu}{2}-\frac{\xi}{2}-ut\right)\right]\right\}, \quad (23a)$$

$$\psi_m=4\tan^{-1}\left\{\exp\left[\sigma\Lambda\left(x-\frac{\mu}{2}+\frac{\xi}{2}-ut\right)\right]\right\}, \quad (23b)$$

$$\varphi_{m-1}=4\tan^{-1}\left\{\exp\left[\Lambda\left(x+\frac{\mu}{2}-\frac{\xi}{2}-ut\right)\right]\right\}, \quad (23c)$$

$$\psi_{m-1}=4\tan^{-1}\left\{\exp\left[\sigma\Lambda\left(x+\frac{\mu}{2}+\frac{\xi}{2}-ut\right)\right]\right\}, \quad (23d)$$

where

$$\Lambda=\gamma\left(\frac{u}{\sqrt{1-\sigma\varepsilon}}\right)\frac{1}{\sqrt{1-\sigma\varepsilon}}.$$

For $\sigma=-1$ $[\sigma=+1]$ Eqs. (23) describe two fluxon-antifluxon pairs (one at m and the other at $m-1$). In the pair, the center of mass of the fluxon is at distance ξ from the center of mass of the antifluxon [fluxon]. The centers of mass of the two pairs are separated by μ, and move with velocity u, as it is shown at top of Fig. 2 [Fig. 3]. For $\xi=\mu=0$, Eqs. (23) describe the building block of the fluxon-fluxon string Eq. (18) or the fluxon-antifluxon string Eq. (19).

Using the solutions Eqs. (23), only the magnetic term of the interaction energy in Eq. (22) can be calculated analytically,

$$E_\varepsilon(\xi)=-\varepsilon\int_{-\infty}^{+\infty}\varphi_{mx}\psi_{mx}dx=-8\Lambda\sigma\varepsilon\frac{(\Lambda\xi)}{\sinh(\Lambda\xi)}, \quad (24)$$

while the other terms must be evaluated numerically. However, we are interested to the stability of a string in which the solitons are exactly aligned ($|\xi|=|\mu|=0$). Therefore, considering small deviation from the alignment ($|\xi|<1,|\mu|<1$), we can obtain an approximate analytic expression for the interaction energy expanding the integrand in Eq. (22) in power series of ξ, μ. To the fourth order in the variables, we find

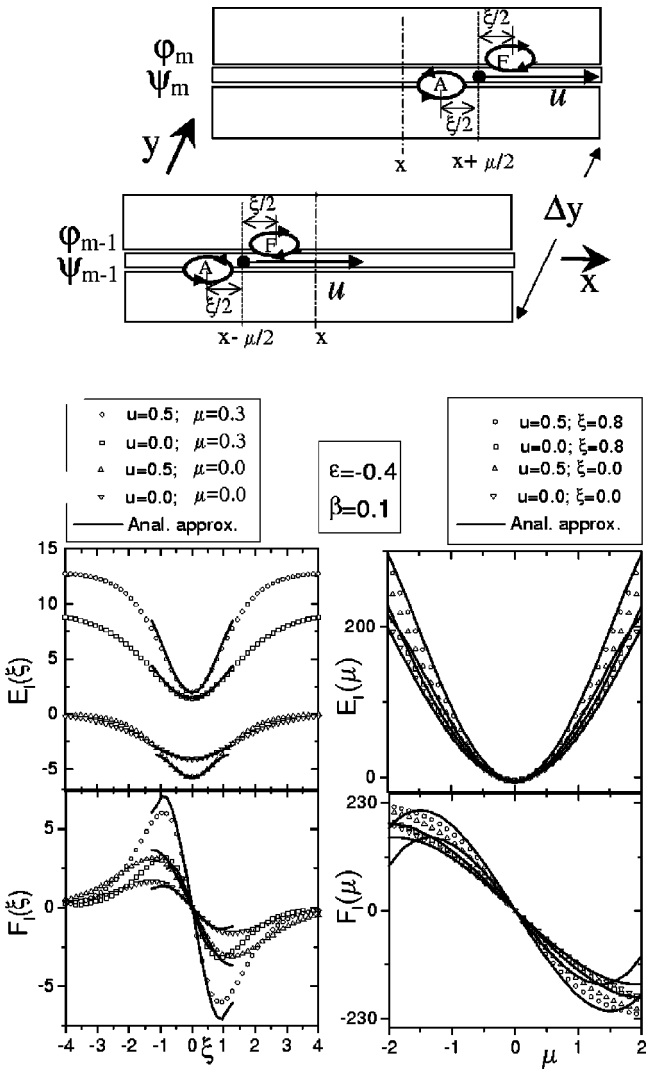

FIG. 2. Top: Nearest-neighbor solitons belonging to a fluxon-antifluxon (F-A) string. Bottom: Interaction energy and interaction force between the fluxon and the antifluxon in a pair (at left), and between the two contiguous fluxon-antifluxon pairs (at right).

$$E_I(\xi,\mu)\approx-\sigma 8\Lambda\varepsilon+\frac{4}{3}\Lambda^3\sigma\varepsilon\xi^2+\frac{8}{\beta}\Lambda(1-\sigma\varepsilon)\mu^2-\frac{7}{45}\sigma\varepsilon\Lambda^5\xi^4+\frac{4}{3}\Lambda^3\frac{\sigma\varepsilon}{\beta}\xi^2\mu^2-\frac{2}{9}\frac{\Lambda^3}{\beta}(1-\sigma\varepsilon)\mu^4. \quad (25)$$

The numerically evaluated interaction energy and interaction force

$$F_I(\xi,\mu)=-\nabla_{\xi,\mu}E_I(\xi,\mu)$$

as well as their analytic approximation are shown in Fig. 2 for the fluxon-antifluxon pairs ($\sigma=-1$) and in Fig. 3 for the fluxon-fluxon pairs ($\sigma=+1$).

Figure 2 shows that the interaction between fluxon and antifluxon in a pair, i.e.,

$$E_I(\xi)|_{\mu=const},$$

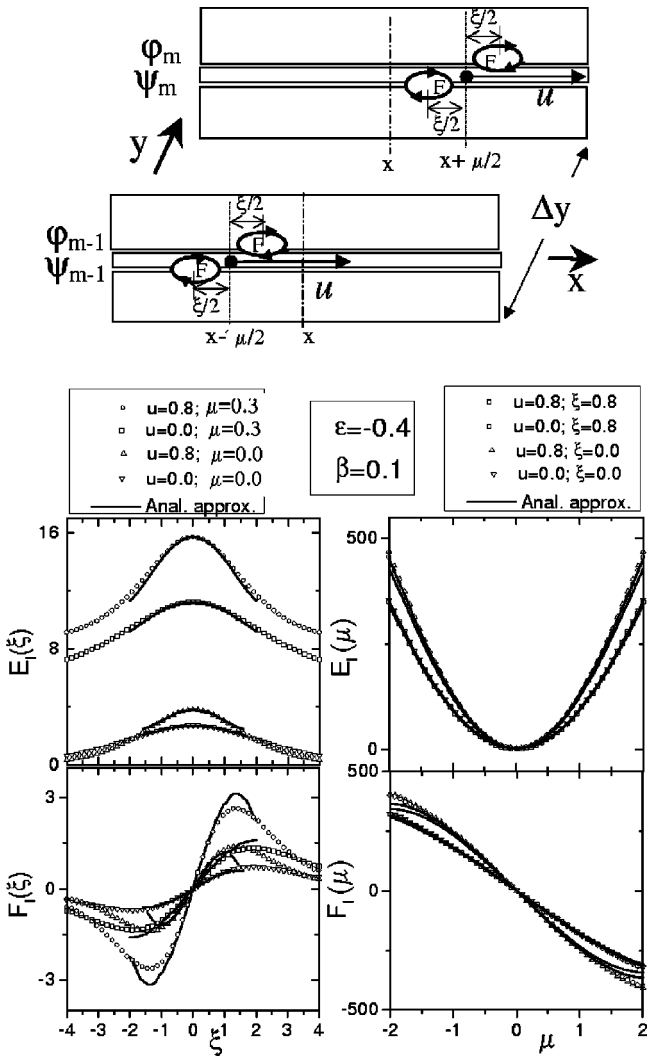

FIG. 3. Same meaning as in Fig. 2, but here fluxon-fluxon pairs are considered.

$$F_I(\xi) = -\frac{\partial E_I}{\partial \xi}\Big|_{\mu=const},$$

is attractive as well as the interaction between two contiguous pairs

$$E_I(\mu)\big|_{\xi=const},$$

$$F_I(\mu) = -\frac{\partial E_I}{\partial \mu}\Big|_{\xi=const}.$$

Conversely, from Fig. 3 we deduce that, though the interaction between two contiguous fluxon-fluxon pairs is attractive, the interaction between the fluxons constituting the pair is repulsive, making impossible to originate a stable string of fluxon-fluxon pairs. We conclude that the stable configuration is the one shown in Fig. 2, or, in other words, that a stable solitonic solution in our system is the fluxon-antifluxon string. In the following we will focus on this state.

2. Modification of basic soliton interactions in the hybrid structure

In the fluxon-antifluxon string the arrangement of solitons can be regarded as the combination of configurations occurring in simpler structures. In particular, the fluxon-antifluxon pair at m (φ_m and ψ_m in Fig. 2) is topologically equivalent to the one observed[12,13] in a single two stack of long Josephson junctions, while the nearest-neighbor fluxons at m and $m-1$ (φ_m and φ_{m-1} in Fig. 2) are topologically equivalent to a couple of homopolar solitons occurring[19] in parallel arrays of long Josephson junctions. It can be interesting to see how the basic interactions between solitons in these simpler structures are modified in our hybrid structure. Restricting ourself to the nonrelativistic regime ($u \ll 1$) and to small departure from the equilibrium point ($|\xi| \ll 1$, $|\mu| \ll 1$), the force $F_I^{(arr)}$ between two fluxons in the parallel array[19] and the force $F_I^{(stack)}$ between the fluxon and the antifluxon in the two stack of single Josephson junctions [where the $E_\varepsilon(\xi)$ is given exactly by Eq. (24)] are

$$F_I^{(arr)}(\mu) = -\frac{8}{\beta}\mu, \tag{26a}$$

$$F_I^{(stack)}(\xi) = -\frac{8}{3}|\varepsilon|(1-|\varepsilon|)^{-3/2}\xi. \tag{26b}$$

The analogous forces in our system are calculated from Eq. (25) as

$$F_I^{(stack-arr)}(\mu)\big|_{\xi=const} = -\frac{1}{2}\frac{\partial E_I}{\partial \mu} \simeq -\left[\frac{8}{\beta}\sqrt{1-|\varepsilon|} + \frac{4}{3}\frac{|\varepsilon|}{\beta} \times (1-|\varepsilon|)^{-3/2}\xi^2\right]\mu, \tag{27a}$$

$$F_I^{(stack-arr)}(\xi)\big|_{\mu=const} = -\frac{\partial E_I}{\partial \xi} \simeq -\left[\frac{8}{3}\left|\varepsilon\right|(1-|\varepsilon|)^{-3/2} + \frac{8}{3}\frac{|\varepsilon|}{\beta} \times (1-|\varepsilon|)^{-3/2}\mu^2\right]\xi. \tag{27b}$$

Notice that

$$\lim_{\varepsilon\to 0} F_I^{(stack-arr)}(\mu) = F_I^{(arr)}(\mu),$$

$$\lim_{\beta\to\infty} F_I^{(stack-arr)}(\xi) = F_I^{(stack)}(\xi),$$

as should be expected, because our two stack of parallel arrays reduces to two uncoupled parallel arrays in the limit of vanishing ε (physically, intermediate electrode thickness d very large with respect to λ_L), or to p uncoupled two-stack of long junctions in the limit of very high β (physically, separation Δy between the junctions very large with respect to λ_J).

From Eqs. (26) and (27) we deduce that in our structure the force between the two fluxons is reduced with respect to that in the single parallel array, while the force between fluxon and antifluxon is increased with respect to that in the single two stack of long Josephson junctions. Moreover, in the hybrid structure the two forces depend, though weakly, on the relative arrangements of solitons (i.e., depend on ξ and μ). This relatively small effect arises from the term $E_{\varepsilon\beta}=\int \overline{H}_{\varepsilon\beta}dx$ in the interaction energy Eq. (22), which is peculiar of the hybrid nature of our structure.

3. I-V curve of fluxon-antifluxon string

Turning to the fluxon-antifluxon string, we can obtain its *I-V* curve using a simple energetic approach. Differentiating with respect to the time the energy Eq. (21) and by using Eqs. (4), we get

$$\frac{dH}{dt}=\int_{-\infty}^{+\infty}dx\Bigg\{\sum_{m=2}^{p-1}(-\alpha\varphi_{mt}^2-\alpha\psi_{mt}^2)+\frac{1}{2}[-\alpha\varphi_{1t}^2-\alpha\varphi_{pt}^2+(p-1)(\gamma_A-\gamma_B)\varphi_{1t}+(p-1)(\gamma_A+\gamma_B)\varphi_{pt}]+\frac{1}{2}[-\alpha\psi_{1t}^2-\alpha\psi_{pt}^2+(p-1)(\gamma_B-\gamma_A)\psi_{1t}+(p-1)(\gamma_A+\gamma_B)\psi_{pt}]\Bigg\}. \tag{28}$$

Following the classic approach,[24] we assume that the dominant perturbation is in the velocity and we assume also the existence of a stationary velocity u that makes the energy stationary. The velocity of the string is then found by inserting the fluxon-antifluxon string solution

$$\varphi_m=4\tan^{-1}\left\{\exp\left[\gamma\left(\frac{u}{u^-}\right)\frac{x-ut}{\sqrt{1+\varepsilon}}\right]\right\}\equiv\phi,$$

$$\psi_m\equiv-\phi,$$

in Eq. (28) with $dH/dt=0$ (power balance) to have

$$2(p-1)\alpha\int_{-\infty}^{+\infty}\phi_t^2dx=(p-1)(\gamma_A-\gamma_B)\int_{-\infty}^{+\infty}\phi_t dx,$$

and hence

$$\frac{\gamma_A-\gamma_B}{2}=\frac{4\alpha}{\pi}\frac{u}{u^-}\frac{1}{\sqrt{1-(u/u^-)^2}}, \tag{29}$$

where $u^-=\sqrt{1+\varepsilon}$.

It is known[4] that the dynamical state of one or more fluxons oscillating in a long Josephson junction is manifested in the *I-V* characteristic of the junction as zero-field current singularities, evenly spaced in voltage, named zero-field steps (ZFS's) and labeled from the lower to higher voltage of appearance as ZFS1, ZFS2, ZFS3, and so forth. The voltage of these singularities is proportional to the mean velocity u of the fluxons, $V_{ZFSN}=uN2\pi/l$, or, in physical units,

$$V_{ZFSN}=N\frac{\Phi_0}{L}u=NV_{ZFS1}, \tag{30}$$

where L is the junction length. If the oscillating solitons are antifluxons moving with the same mean velocity u, a similar picture is obtained, but for the voltage polarity. Here, the fluxon-antifluxon string consists of p fluxons in one array (e.g., the φ_m array) and p antifluxons in the other array (e.g., the ψ_m array). Since the voltages across the two arrays are measured in parallel, the same values as from two single junctions are expected to be measured. In other words, using the same notation as for the single junctions, voltages

$$V_A^{(ZFSN)}=-V_B^{(ZFSN)}=N\frac{\Phi_0}{L}u \tag{31}$$

are expected if N fluxon-antifluxon strings are oscillating in the system with mean velocity u.

From Eq. (31), and noticing that γ_A and γ_B are proportional to the physical bias currents, $\gamma_{A,B}=I_{A,B}/J_0LW$, Eq. (29) should describe the *I-V* curve of the ZFS's accounting for fluxon-antifluxon strings oscillating in the two stack of parallel arrays of long Josephson junctions.

III. NUMERICAL RESULTS

We investigated numerically the excitation of the cavity mode resonances as well as the fluxon-antifluxon strings in the structure integrating the full system of coupled perturbed sine-Gordon equations Eqs. (4). For what concerns the linear modes, we first analyze the results obtained with a magnetic field applied in the y direction, i.e., $\eta^E\neq0$ and $\eta^T=0$, and then we analyze the results with respect to the application of a magnetic field in the x direction, both in the case of a field externally applied ($\eta^T\neq0$) and in the case of the self-field generated by the bias currents. The *I-V* curve of the fluxon-antifluxon string is then indagated at $\eta^E=\eta^T=0$.

A. Cavity modes excited by a magnetic field in the *y* direction: Two-dimensional synchronized oscillations

In the main plot of Fig. 4 it is shown the calculated *I-V* characteristic $\gamma_A(V_A)$ of a five-junction array ($p=5$) of a two stack, while the other array is unbiased ($\gamma_B=V_B=0$). The plot is obtained superimposing the curves calculated at different magnetic fields ranging between $\eta^E=6.0$ and $\eta^E=7.5$. As it is seen in the plot, the cavity modes excited by a magnetic field in the y direction manifest themselves as two series of current singularities with characteristic voltage spacings ΔV_{FS}^- and ΔV_{FS}^+. As discussed in the previous section, these two voltage spacings correspond to the two possible velocities u^- and u^+ for linear (electromagnetic) waves in the structure. The vertical bars in the plot indicate the voltage positions of the resonances as predicted by Eq. (10). The snapshots show the instantaneous voltage profiles $[\varphi_{nt}(x,t_0),\ \psi_{nt}(x,t_0)]$ of all the junctions in the two stack when we are biasing the arrays on a Fiske step of the u^- or of the u^+ family. As it is seen, the voltage profiles along the x direction are nearly cosinusoidal in form and in phase in each of the arrays. Moreover, the voltage profiles of the bottom and of the top array are out of phase for the Fiske in the u^- family or in phase for the Fiske in u^+ family, in qualitative agreement with the prediction of the spatial voltage profiles given by Eq. (11).

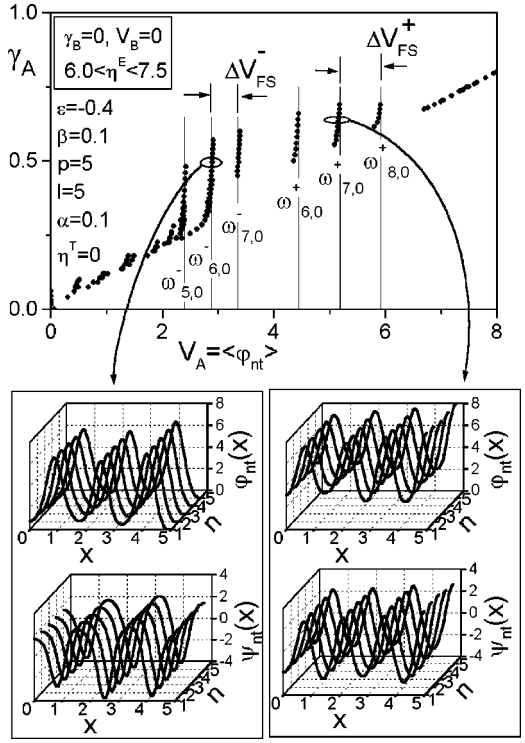

FIG. 4. Calculated *I-V* characteristic of the cavity mode resonances excited by a magnetic field in the *y* direction, as recorded in the top array of the two stack while the bottom array is unbiased. The vertical bars are the asymptotic voltages of the singularities as predicted by Eq. (10). The snapshots freeze the instantaneous voltage profiles of the junctions when the two stack is biased on the singularities.

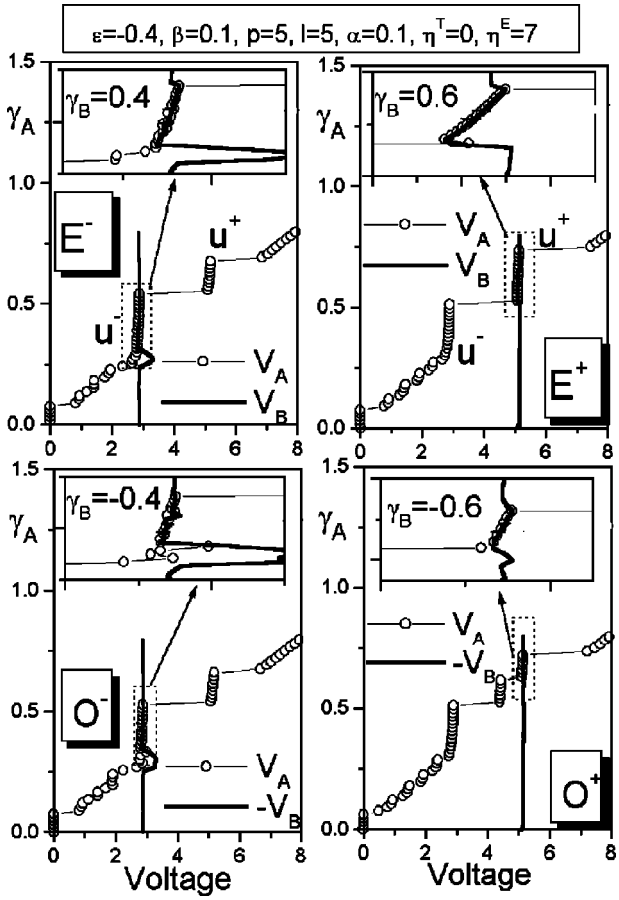

FIG. 5. Numerical voltage locking on Fiske steps of the u^- and u^+ family. The locking is with equal voltage polarities (E^- and E^+ states) if bias currents of the same polarities are used, or with opposite voltage polarities (O^- and O^+ states) if bias currents of opposite polarities are used.

From results in Fig. 4 we deduce that it is not necessary to bias the arrays with equal currents to excite cavity modes in the structure. In the reported example we did not bias the bottom array, with the result of oscillations surfing on a zero mean voltage ($V_B=0$) and oscillations in the top array surfing on a finite mean voltage ($V_A\neq 0$). Due the coupling terms present in system Eqs. (4) we could expect that, if not so different currents were used, both the synchronization of the ac components and a locking between the mean voltages of the arrays could be established. The results of a numerical voltage locking calculation are summarized in Fig. 5. To identify the current range where voltage locking is achieved, we plotted on the same graph the voltage of both the arrays as a function of the variable current [$\gamma_A(V_A)$ and $\gamma_A(V_B)$ in Fig. 5]. As shown in the numerical results, we can excite voltage locked states in the u^- family of Fiske steps, with equal or opposite voltage polarities (E^- and O^- states in Fig. 5), as well as in the u^+ family (E^+ and O^+ states in Fig. 5). From numerical simulations it is found that voltage locked states in the u^+ family consist of in-phase cavity modes and the voltage locked states in the u^- family consist of out-of-phase cavity modes, whose spatial voltage profiles are similar to the ones shown in Fig. 4 and again approximately described by Eq. (11).

We should remark that the E^+ and O^+ states are an example of synchronization both in the *y* direction (adjacent junctions in one array are synchronized) and in the *z* direction (junctions of the bottom array are synchronized with junctions of the top array) of the structure. Moreover, these two-dimensional (2D) synchronized linear oscillations have equal amplitudes, a good feature for what concerns possible microwave applications.

Due to the in-phase nature of the modes, the amplitude of the ac signal [see Eq. (11)] expected from the structure is proportional to $2p$ times the amplitude of the ac signal from a single junction. As it is known, the oscillation frequencies in real junctions are in the microwave range, so our structure, when operated in the E^+ or O^+ states, could be of interest as a microwave oscillator.

B. Cavity modes excited by a magnetic field in the *x* direction

In the main plot of Fig. 6 are shown numerical *I-V* curves of the cavity modes excited by a magnetic field in the *x* direction. Same general representation as in Fig. 4 has been adopted to represent the cavity modes. Here the magnetic field in the *x* direction is varied between $\eta^T=7$ and $\eta^T=10$, and we put $\eta^E=0$, and $\gamma_A=\gamma_B$. The vertical bars are the asymptotic voltage positions of the current singularities as predicted by Eq. (12). A satisfactory agreement with predictions of Eq. (12) was found also for other β values, as it is seen in the inset of Fig. 6. In the snapshots we report the voltage profiles of the junctions corresponding to the first cavity mode resonances of the u^- and u^+ family. The volt-

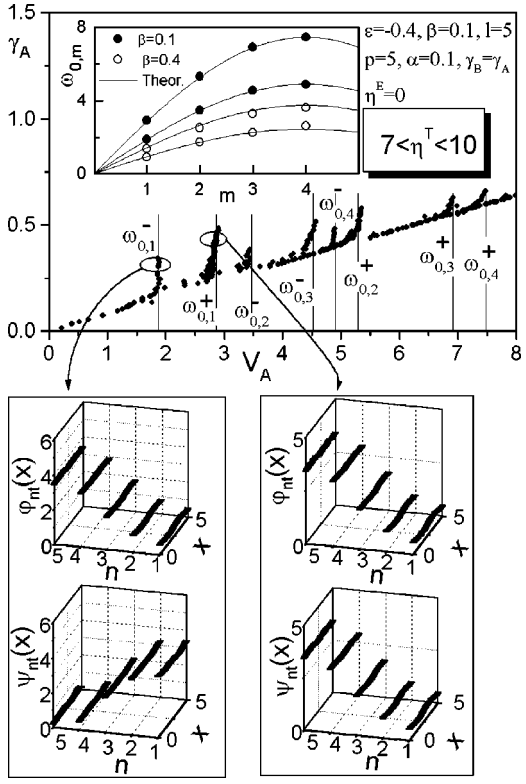

FIG. 6. Calculated *I-V* curves of the cavity mode resonances excited by a magnetic field in the *x* direction, as recorded in the top array of the two stack. The vertical bars are the asymptotic voltages of the singularities as predicted by Eq. (12). In the inset the values of the asymptotic voltages numerically obtained for two different discreteness parameters β are compared with the ones expected by Eq. (12). The snapshots froze the instantaneous voltage profiles of the junctions when they are biased on the marked singularities.

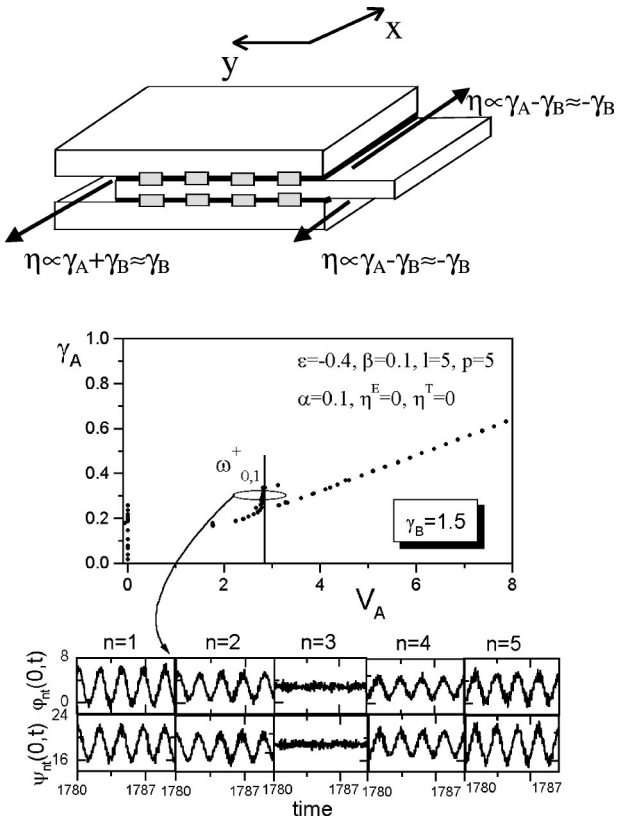

FIG. 7. Top: Magnetic field (self-field) in the *x* direction due to the bias currents. Center: A cavity mode resonance excited using the self-field generated biasing the bottom array with $\gamma_B \gg \gamma_A$ in the absence of an externally applied magnetic field ($\eta^T=0$). Bottom: Voltage signals at one edge of the two stack when it is biased on the resonance.

age profiles of the bottom array and of the top array are found out-of-phase for the mode in the u^- family and in-phase for the mode in the u^+ family. Moreover, a vanishingly small spatial modulation along the *x* direction and an amplitude modulation of the voltages along the discretized direction is recorded, as qualitatively expected by Eq. (13).

1. In-phase cavity modes excited without external magnetic field

Due to the configuration of the electrodes in our structure [see Fig. 1(b)], a current passing through one array of the stack generates a magnetic field in the *x* direction that enters the loops of the other array. In other words, a magnetic field in the *x* direction can be applied using a solenoid or by means of the self-fields generated by the current biasing the structure. This peculiar feature of our hybrid structure is captured by the mathematical description, Eqs. (4), of the system, since the η^T term accounting for the external magnetic field and terms proportional to the bias currents γ_A and γ_B play a similar role. This is clearly seen also in the model Eqs. (1) of the continuous version of our structure [see Fig. 1(a)] where the self-fields play in the boundary conditions a role similar to the external magnetic field η^T. It follows that, if we bias the bottom array of the two stack with a current γ_B sufficiently high and if $\gamma_B \gg \gamma_A$, this results in a field applied along the *x* direction and proportional to γ_B, as it is shown at the top of Fig. 7. Such a self-field, though asymmetrical, is expected to excite cavity mode resonances described by Eqs. (12) and (13). This is confirmed by numerical results, as it is shown in Fig. 7, where with $\eta^T=0$ and $\gamma_B=1.5$ we excited the same $\omega^+_{0,1}$ resonance shown in Fig. 6, where $\omega^+_{0,1}$ was excited for $\eta^T=7$. From the time evolution of the voltage signals at one edge of the two stack for the $\omega^+_{0,1}$ shown at bottom of Fig. 7 we see that the ac voltage signals in the two arrays are found to be again described by Eq. (13).

2. Analysis of microwave signals at one edge of the structure from $\omega^{\pm}_{0,m}$ resonances

For what concerns the possible interest of the structure as a microwave oscillator, it could be interesting to know from which resonances of the $\omega^{\pm}_{0,m}$ series a large ac signal can be expected if all the signals from the single junctions were superimposed and conveyed from one edge of the structure. The inspection of the amplitude distribution of the ac signals predicted by Eq. (13) indicates that the resonances of the u^- family are inadequate to this purpose, because of the cancellation of signals from bottom and top array for each *n*. In the u^+ family the signals from the bottom array add with same sign to the signals from the top array, but signals of the same array can add destructively. For example, for $p=5$ case, the total voltage signal $\sigma_A(t)=\Sigma_n \varphi^{(ac)}_{nt}$ associated to the top array and the total signal $\sigma_B(t)=\Sigma_n \psi^{(ac)}_{nt}$ associated to the bottom array are both zero for the odd resonances ($\omega^+_{0,1}$ and

$\omega^{+}_{0,3}$), while the signal of only one junction emerges from the top and the signal of only one junction emerges from the bottom array when the two stack is operated on an even resonance ($\omega^{+}_{0,2}$ and $\omega^{+}_{0,4}$).

We remark that in simpler structures, as the ordinary long Josephson junction, the radiation normally coupled out from one edge of the junction is substantially of electric nature. When seen as a resonant cavity, a magnetic field applied perpendicular to the long dimension (in our notation, a field applied along the *y* direction) excites cavity modes where the electric field has a maximum at the edges, while the magnetic field has a node at the edges of the junction. In this case the analysis of the temporal derivative of the phase at one edge of the junction, proportional to the electric field, is what matters. In this sense, the analysis we made in the previous section on the voltage signals at one edge of the two stack in correspondence of Fiske modes excited by a magnetic field in the *y* direction is the analysis relevant for applications. On the other hand, when we apply a magnetic field in the *x* direction and we want again to couple the signals from all junctions at the $x=0$ edge of the two stack, we should analyze also the magnetic component of the signals along the *y* (discretized) direction, because in this case it is not zero.

In the two-dimensional stack in Fig. 1(a) the nontrivial components of the fields in the top junction are related to the phase derivatives as[21]

$$^{(\varphi)}E_z(x,y,t) \propto \varphi_t(x,y,t), \tag{32a}$$

$$^{(\varphi)}B_y(x,y,t) \propto \varphi_x(x,y,t) - \varepsilon \psi_x(x,y,t), \tag{32b}$$

$$^{(\varphi)}B_x(x,y,t) \propto -[\varphi_y(x,y,t) - \varepsilon \psi_y(x,y,t)], \tag{32c}$$

and similarly for the bottom junction. In our discrete structure, the ac component of the electric field at the $x=0$ edge (see bottom of Fig. 8) are

$$^{(\varphi)}E_z^{(ac)}[n] \propto \varphi_{nt}^{(ac)}(x=0,t), \tag{33a}$$

$$^{(\psi)}E_z^{(ac)}[n] \propto \psi_{nt}^{(ac)}(x=0,t). \tag{33b}$$

From these relations, an analysis of expected total signal based on relation (13) is, indeed, an analysis of the ac electric field.

To evaluate the magnetic fields of interest, i.e., $^{(\varphi)}B_x(x=0)$, we first notice that Eqs. (32a) and (32b) can be simplified when we are concerned with a cavity mode. For the cavity modes of the u^{+} family, which we are interested in, is $\varphi^{(ac)} = \psi^{(ac)}$, so that we can work with the simplified relations

$$^{(\varphi)}B_x(0,y,t) \propto -\varphi_y(0,y,t), \tag{34a}$$

$$^{(\psi)}B_x(0,y,t) \propto -\psi_y(0,y,t). \tag{34b}$$

We can now substitute the partial derivative with respect to *y* in Eqs. (34) with the approximated finite differences to obtain for the ac components of the magnetic field

$$^{(\varphi)}B_x^{(ac)}[n] \propto -(\varphi_{n+1}^{(ac)} - \varphi_n^{(ac)}), \tag{35a}$$

$$^{(\psi)}B_x^{(ac)}[n] \propto -(\psi_{n+1}^{(ac)} - \psi_n^{(ac)}). \tag{35b}$$

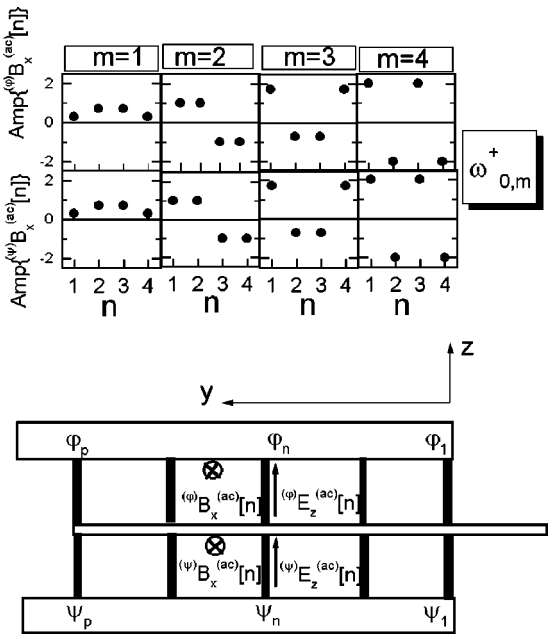

FIG. 8. Magnetic and electric fields of interest at one edge of the two stack (bottom) and (top) expected amplitude distribution of the ac component of the magnetic field when a cavity mode of the $\omega^{+}_{0,m}$ series is excited.

The amplitudes of the ac component of the magnetic field evaluated using Eqs. (35) and (13) for the $\omega^{+}_{0,m}$ resonances are shown at the top of Fig. 8. The inspection of Fig. 8 indicates that now, in contrast to the electric case, the total magnetic signals are relevant for the odd resonances, while they cancel out in the even resonances. Moreover, comparable total signals are expected from consecutive odd resonances. We conclude that for the odd resonances a magnetic contribution from all the junction of the arrays is expected.

Taking into account also the previous discussion on the electric components, we can conclude that the total ac signal from one edge of a two stack operated on the resonance excited by a magnetic field in the *x* direction is zero from the $\omega^{-}_{0,m}$ resonances and other than zero from the $\omega^{+}_{0,m}$ resonances. This signal is of electric nature for the even resonances and of magnetic nature for the odd resonances. The magnetic signal is expected to be larger than the electric signal.

C. Fluxon-antifluxon string

In Fig. 9 it is shown the numerical *I-V* characteristic of the ZFS1 (first zero field step) seen in one array of the stack while the other is biased with constant current. In the same figure, the snapshot of the voltage freezes, as we should expect, a fluxon-antifluxon string that is oscillating with mean velocity *u* in the two stack. The analytic *I-V* curve Eq. (29) is also reported for comparison. We found that the agreement with the numerical curves is satisfactory for $l=20$, while an evident deviation is seen for $l=5$, $\gamma_B=0$. This is not surprising if we consider the physical interpretation of the results of the mathematical model.

In fact, if we depict the solitonic dynamics of the fluxon-antifluxon pairs constituting the string in terms of the motion of two particles in a bound state, the half difference of the

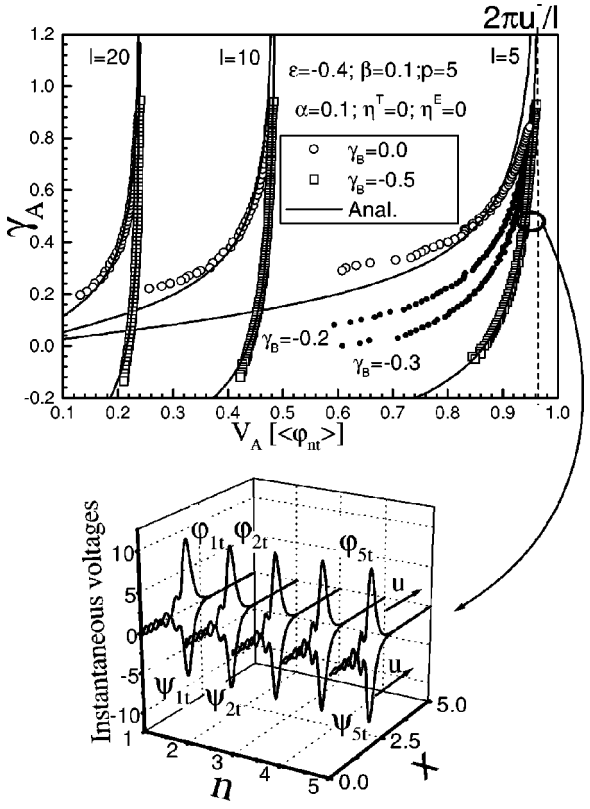

FIG. 9. Numerical (points) and theoretical (solid lines) *I-V* curves of the ZFS1 for different lengths of the two stack. In the snapshot are shown the instantaneous voltage profiles of the junctions when the two stack is biased at the marked point of the ZFS1.

bias currents gives the net Lorentz force acting on the center of mass, while the half sum can be seen as a force opposing the internal attractive force between the antipolar solitons. If the bias currents are not so different to break the pairs, the internal motion consists of damped harmonic oscillations around the centers of mass of the bound states. On this basis, the assumption of perfect (aligned and rigid) fluxon-antifluxon string is well justified when $\gamma_B = -\gamma_A$, while it is only marginally justified when, as in our numerical steps in Fig. 9, $\gamma_B = 0$. Moreover, when we assumed infinite length junctions in the derivation of Eq. (29), we implicitly neglected the finite size of the solitons, which is obviously relevant when the junctions are not very long (as in the case of $l = 5$ of Fig. 9).

We observe in Fig. 9 oscillations in the fluxon tails, a phenomenon well known in numerical simulations of single long Josephson junctions.[22] As in the single junctions, also here the amplitude of the oscillations grows as the length of the junctions is shortened, or the fluxons are pushed closer to the limit velocity. In both cases the solutions assumed in perturbative theory lose their validity. Here, a further deviation from simple theory arises from the internal degree of freedom (oscillations around the centers of mass) and the general complexity of the system.

IV. EXPERIMENT

We have fabricated and tested two stacks of parallel arrays of long $Nb/AlO_x/Nb$ Josephson junctions with the geometry shown in Fig. 1(b). The fabrication process we used is similar to the one used in Ref. 13. The two stacks have $\approx 300-$nm thick outer electrodes and $\approx 90-$nm thick intermediate electrodes. The critical current density per junction in the arrays (as estimated from the current rise at the gap sum voltage) was mostly found to be ≈ 70 A/cm$^2 \pm 10\%$. In the three samples on which we report here, the arrays of the two stack have five ($p = 5$) junctions with physical dimensions $L \times \delta = (600 \times 20)$ μm^2 separated by $\Delta y = 20$ μm. For all the samples the critical current of the arrays (as measured at $V = 0$) are $I_{cA} \approx I_{cB} = 20$ mA. We estimate Josephson penetration lengths $\lambda_{JA} \approx \lambda_{JB} = 60$ μm, normalized lengths $l_A \approx l_B = 10$, and discreteness parameter $\beta \approx 0.1$. From the thickness of the intermediate electrode a magnetic coupling of the order of $\varepsilon = -0.5$ is expected from relation (2). Finally, the critical field is estimated to be $B_c \approx 0.1$ G.

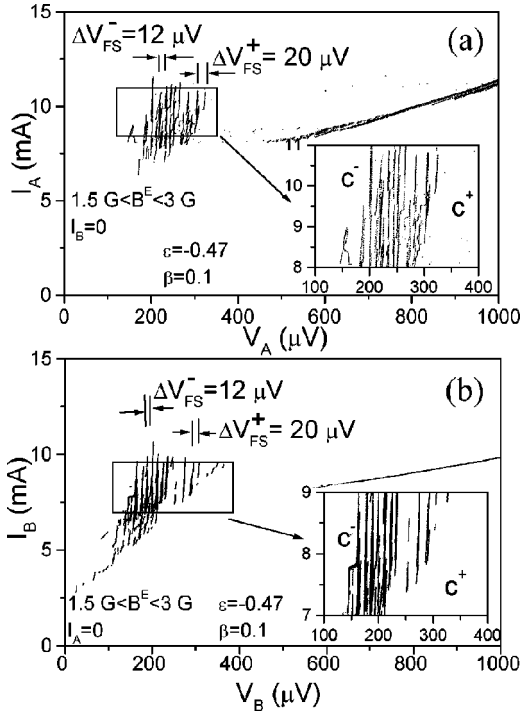

FIG. 10. Cavity modes resonances in the top [(a)] and in the bottom [(b)] array of a two stack excited by a magnetic field in the *y* direction. Here $\varepsilon = -0.47$ is estimated.

A. Cavity mode resonances: experimental evidence for 2D synchronized state

Figure 10 shows the cavity modes resonances (or Fiske steps) excited in one array of a two stack by a magnetic field in the *y* direction, while the other array is unbiased. The cavity modes exhibit two characteristic voltage spacings $\Delta V_{FS}^{-} \approx 12$ μV and $\Delta V_{FS}^{+} \approx 20$ μV. As noted above [see Eq. (14)], this phenomenon arises from the splitting of the Swihart velocity $\bar{c}$ in two velocities $\bar{c}^{+}$ and $\bar{c}^{-}$ corresponding to an in-phase oscillation or to an out-phase oscillation mode, as it is shown in the numerical results of Fig. 4. From data in Fig. 10 and relation (14) we estimate for this two stack a magnetic coupling $\varepsilon = -0.47$. With similar procedure $\varepsilon = -0.49$ and $\varepsilon = -0.60$ are estimated in the other investigated two stacks. The observed values agree with $\varepsilon = -0.5$ expected from Eq. (2).

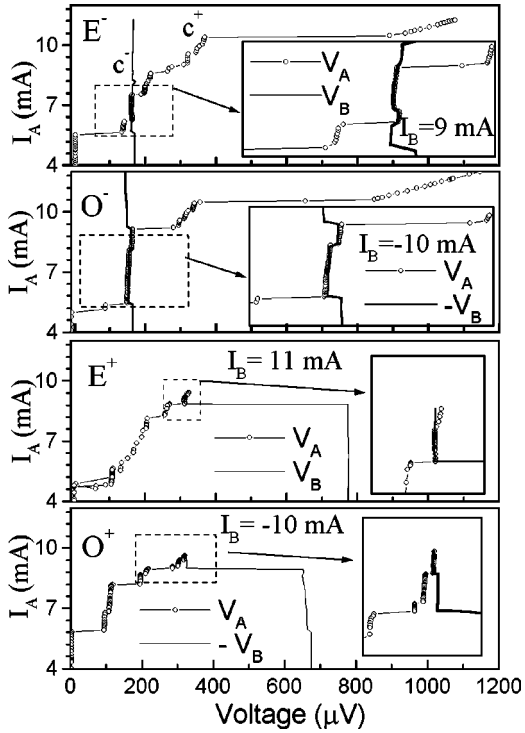

FIG. 11. Voltage locked Fiske modes recorded in the two-stack with $\varepsilon=-0.47$. The magnetic field is $B^E=2$ G.

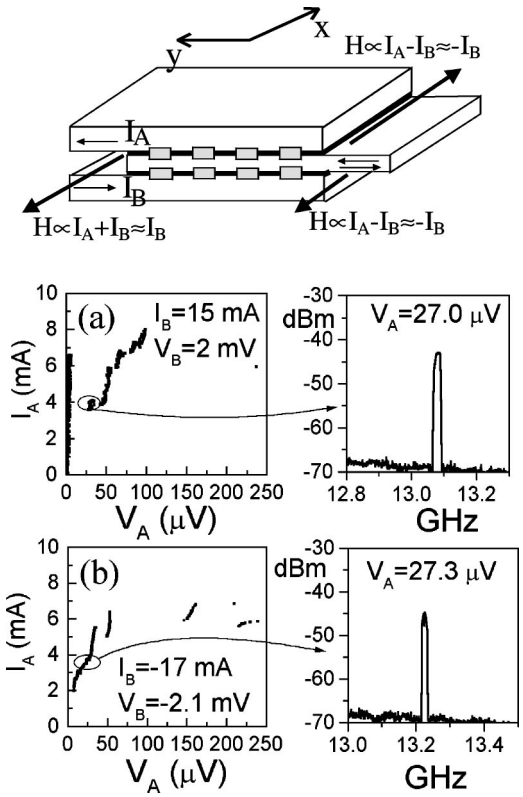

FIG. 12. Microwave radiation received by cavity modes excited in the top array of the two stack with $\varepsilon=-0.47$ biasing the bottom array with a positive [in (a)] or negative [in (b)] current. The resonances are induced by the self-field in the x direction associated to the rather large current flowing in the bottom array, as shown in the top of the figure.

Biasing one array of the stack with a constant current and sweeping the other on the Fiske steps, up to four voltage locked states can be recorded. In other words, four different Fiske modes can be excited, with equal or opposite voltage polarities, belonging to the $\overline{c^-}$ as well as to the $\overline{c^+}$ family. This is shown in Fig. 11, where we labeled as $O^{\pm}$ the voltage locked states with opposite voltage polarities and as $E^{\pm}$ the voltage locked states with equal voltage polarities. As noted for numerically obtained voltage locked states in Fig. 5, the E^- and O^- states consist of an out-of-phase oscillation of the instantaneous voltage profiles of the two arrays, while the E^+ and O^+ states consist of an in-phase oscillation. Data in Fig. 11 refer to the two stack with $\varepsilon=-0.47$; similar results were obtained for the other investigated devices.

The voltage locked states in Fig. 11 are resembling the ones observed[11] in two stacks of single long Josephson junctions, but here an array of long Josephson junctions plays the role of the single junction in the experiments reported in Ref. 11. As noted in Sec. III, the observed E^+ and O^+ states consist of modes where the adjacent junctions of both the arrays in the two stack as well as the bottom and the top arrays oscillate in phase. In other words, the structure experimentally exhibits the desired 2D synchronization in both the y and z direction. This should compel a great enhancement of the emitted radiation.

From the Josephson relation $\nu_{\rm em}=\Phi_0^{-1}V$, it follows that the frequency of the emitted signal falls in the range $70<\nu_{em}<200$ GHz for the voltage-locked states reported in Fig. 11. Unfortunately, this frequency range is out of the band of our instrumentation. However, voltage locked states corresponding to frequencies up to $\nu_{em}\approx 400$ GHz were recorded in our samples, and also higher frequencies could be expected [see Eq. (14)] choosing a physical length of the junctions shorter than $L=600$ μm used in the present work. Moreover, using for a single junction in the structure the same parameters as those of the Josephson submillimeter wave tunable local oscillator,[25] a power enhancement proportional to the square of the number of junction in the two stack [i.e., $(2p)^2$] could be obtained for such oscillators if our structure were operated in the E^+ state.

We did not experimentally investigate the cavity mode resonances excited directly by an external magnetic field in the x direction. However, some of these resonances have been excited using the self-fields of one array of the stack as a magnetic field in the x direction, as shown at the top of Fig. 12. In Figs. 12(a), and (b) we show some of the steps recorded in the top array of the two stack with $\varepsilon=-0.47$ obtained by feeding a large current through the bottom array of the stack. As discussed in the previous section (see Fig. 7), the ac component of the voltage signals associated to these resonances is similar to the one obtained by means of an external magnetic field in the x direction. Some of the resonances emit in the band of our instrumentation. In Fig. 12 we report the radiation recorded with a room-temperature spectrum analyzer when the array is biased on the first resonance of the $\overline{c^+}$ family, i.e., $\omega_{0,1}^+$. The radiation was conveyed to a 50-Ω coaxial cable by means of a microstrip line weakly coupled through a capacitive gap to one edge of the two stack. The coupled radiation was found about 50 nW on a 50-Ω unmatched load. As discussed in the previous section,

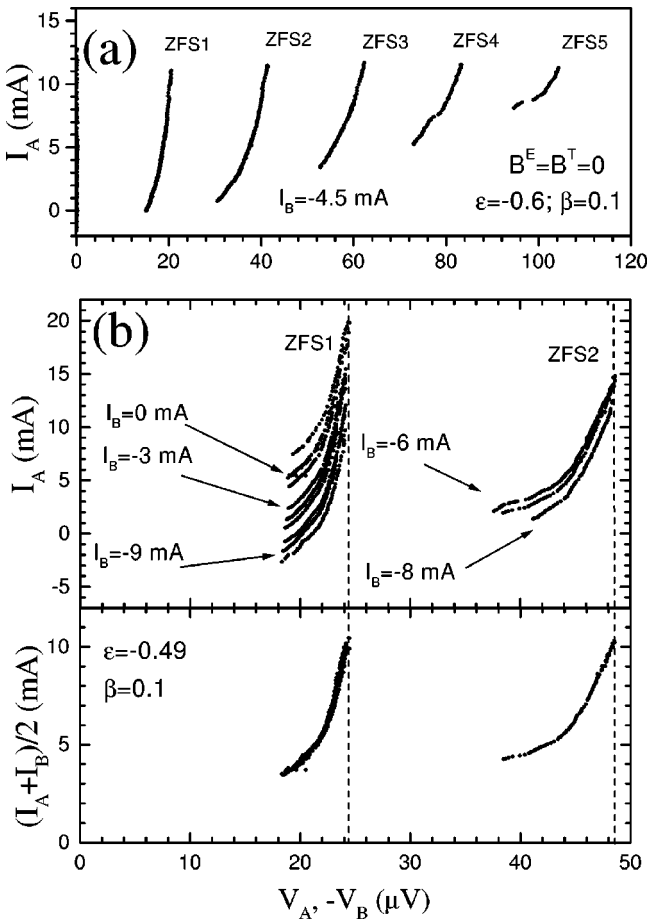

FIG. 13. (a) ZFS's recorded from the top array of a two stack with $\varepsilon=-0.6$ while the bottom array is biased with a negative constant current. (b) I-V characteristics of the ZFS1 and ZFS2 from the top array of a stack with $\varepsilon=-0.49$ using the current biasing the bottom array as a parameter. The curves fall on the top of each other when they are replotted using a current axis defined by: $I_e=(I_A-I_B)/2$.

the radiation coupled from an $\omega_{0,1}^{+}$ resonance is of magnetic nature and, due to the in-phase nature of the mode, it is really expected to be appreciable.

B. Experimental evidence for the fluxon-antifluxon strings

In the absence of magnetic field, by sweeping the bias current of either of the two arrays in the lower region of the McCumber curve while the other array is biased with constant current on the zero voltage state or on the McCumber curve, it is possible the transition to a state where the junctions exhibit voltages having the same magnitude but opposite polarities. When the junctions are in this state, a variation of the bias current in one array results into a variation of the common voltage value (voltage locking); this state exists for a finite range of the bias currents (current steps).

In Fig. 13(a) there are shown five of such current steps, that we named zero-field steps (ZFS's), recorded in the top array of the two stack with $\varepsilon=-0.60$, while the bottom array is biased with a negative constant current. In Fig. 13(b) we report the I-V curves of the ZFS1 and ZFS2 seen in the top array of the stack with $\varepsilon=-0.49$ using the current in the bottom array as a parameter. As the current in the bottom array is increased, the curves shift down. All the curves essentially fall on the top of each other if represented in terms of an ''effective current'' $I_e=(I_A-I_B)/2$.

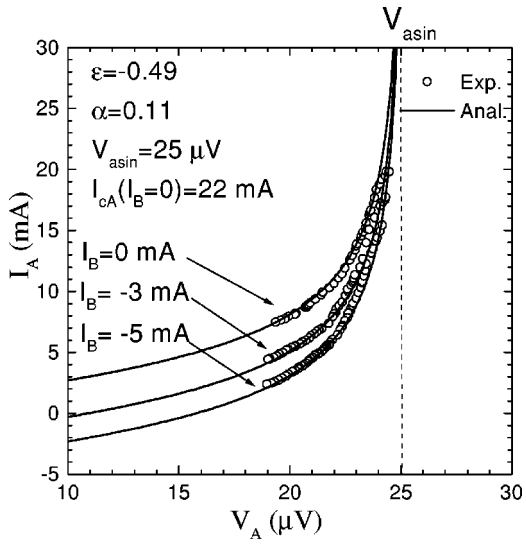

FIG. 14. The experimental I-V characteristics of the ZFS1 in the stack with $\varepsilon=-0.49$ are plotted together with the power balance curves Eq. (29).

The asymptotic voltage of the ZFS1 is $V_{ZFS1}=20.0$ μV in the stack with $\varepsilon=-0.60$ and $V_{ZFS1}=24.0$ μV in the stack with $\varepsilon=-0.49$. These voltage spacings are twice the voltage spacings of the Fiske steps of the c^- family in the two-stacks, as we should expect for an oscillatory motion of solitons with asymptotic velocity c^- [see Eq. (30)]. The global picture, also taking into account the voltage polarities observed [see Eq. (31)], indicates that the we are concerned with one oscillating fluxon-antifluxon string in the ZFS1, two oscillating fluxon-antifluxon strings in the ZFS2, and so on. In other words, we consider the data in Fig. 13 as the experimental evidence for the fluxon-antifluxon strings discussed in the previous sections.

The ZFS's in Fig. 13 show a behavior similar to the ones observed[12,13] in two stacks of single long Josephson junctions. However, here a string of fluxon-antifluxon pairs plays the role of a single fluxon-antifluxon pair in the experiments reported in Refs. 12 and 13. In other words, in the present structure locking between two solitons is extended to $2p$ solitons, with consequently enhanced robustness of the coherent state.

Though obtained assuming a perfect fluxon-antifluxon string and infinite length junctions, the power balance curve Eq. (29) accounts for the major features of the experimental I-V curves. In fact, Eq. (29) predicts u^- (in physical units: c^-) as the asymptotic velocity of the steps and the shift of the I-V curves if the bias current of one of the two arrays is varied as a parameter. Moreover, from Eq. (29) it is evident that the force driving the state is the half difference between the currents, or, in other words, that the curves must fall on the top of each other if represented using an effective current axis defined by the half difference of the currents. An example of fitting the experimental I-V curve of the ZFS1 with the power balance curve is given in Fig. 14.

V. CONCLUSIONS

We have investigated a structure consisting of a two stack of parallel arrays of long Josephson junctions. A model for this system has been derived starting from the description of its continuous limit, i.e., a two stack of two-dimensional Josephson junctions.

Linear wave analysis has shown that, as in the simpler two stack of single Josephson junctions, there exist two characteristic velocities $\overline{c}^{-}$ and $\overline{c}^{+}$ for the propagation of electromagnetic waves in the structure. However, the dispersion relation from electromagnetic waves is found to be a hybrid of the ones exhibited in continuous and discrete systems. The excitation of cavity mode resonances in the structure has been analyzed from analytic point of view and further discussed with the help of numerical simulations. Continuous Fiske modes exhibiting full synchronization in two dimensions ($\omega_{j,0}^{+}$ resonances) and discrete in-phase Fiske modes ($\omega_{0,m}^{+}$ resonances) have been recovered. The $\omega_{0,m}^{+}$ resonances have been found excitable also without external magnetic field. The total electromagnetic signal expected from relevant $\omega_{j,0}^{+}$ and $\omega_{0,m}^{+}$ resonances has been discussed. The total signal expected at one edge of the structure operated in any $\omega_{j,0}^{+}$ resonance is of electric nature and proportional to the total number of junctions $(2p)$, while the signal expected from $\omega_{0,m}^{+}$ resonances is appreciable only for odd resonances, with magnetic nature.

Nonlinear wave analysis has indicated that the basic solitonic solutions of the coupled sine-Gordon equations modeling the system are a fluxon-fluxon string, moving with asymptotic velocity $\overline{c}^{+}$, or a fluxon-antifluxon string, moving with asymptotic velocity $\overline{c}^{-}$. The fluxon-antifluxon string has been proved to be the stable solution considering the interaction energy between the solitons constituting the strings. Moreover, the basic solitonic interactions in the hybrid structure has been compared with the ones in simpler structures, with the result that the attractive interaction of the fluxon-antifluxon pair is increased with respect to that in two stack of single junctions while the fluxon-fluxon interaction is reduced with respect to that in parallel arrays of long junctions. The expected form of the *I-V* curve accounting for the oscillatory motion of a fluxon-antifluxon string along the length of the two stack has been then derived using the power balance approach. The validity of the theoretical *I-V* curve has been discussed with the help of numerical simulations.

The excitation of linear and nonlinear modes has been experimentally demonstrated in two stacks of five-junction arrays. In particular, the two more desired excitations expected in the hybrid structure, namely the 2D synchronized Fiske modes and the 2D phase-locked solitonic mode (fluxon-antifluxon string) have been experimentally demonstrated stable in the structure. Their *I-V* curves as well as microwave radiation received from some cavity mode have been found in agreement with the theoretical and numerical predictions.

ACKNOWLEDGMENTS

The authors wish to thank M. Cirillo, Università di ''Tor Vergata,'' Italy, who provided the photomasks used to fabricate the device. They also acknowledge stimulating discussions with N. F. Pedersen, DTU, Denmark. One of the authors, G. Costabile, wishes to thank the Technical University of Denmark, Lyngby, Denmark, for the warm hospitality. This work was partially supported by a MURST COFIN98 program (Italy).

[1] A. Barone and G. Paternó, *Physics and Applications of the Josephson Effect* (John Wiley & Sons, New York, 1982).
[2] M. Cirillo, N. Grønbech-Jensen, M. R. Samuelsen, M. Salerno, and G. Verona Rinati, Phys. Rev. B **58**, 12 377 (1998).
[3] R. D. Parmentier, in *Solitons in Action*, edited by K. Lonngren and A. C. Scott (Academic Press, New York, 1978).
[4] S. Pnevmatikos and N. F. Pedersen, in *Future Directions of Nonlinear Dynamics in Physical and Biological Systems*, Vol. 312 of *NATO Advanced Study Institute, Series B: Physics*, edited by P. L. Christiansen, J. C. Eilbeck, and R. D. Parmentier (Plenum Press, New York, 1993).
[5] S. Sakai, P. Bodin, and N. F. Pedersen, J. Appl. Phys. **73**, 2411 (1993).
[6] N. Grønbech-Jensen, M. R. Samuelsen, P. S. Lomdahl, and J. A. Blackburn, Phys. Rev. B **42**, 3976 (1990).
[7] N. Grønbech-Jensen, D. Cai, A. R. Bishop, A. W. C. Lau, and P. S. Lomdahl, Phys. Rev. B **50**, 6352 (1994).
[8] N. Grønbech-Jensen, J. A. Blackburn, and M. R. Samuelsen, Phys. Rev. B **53**, 12 364 (1996).
[9] A. V. Ustinov, H. Kohlstedt, and C. Heiden, Appl. Phys. Lett. **65**, 1457 (1994).
[10] S. Sakai, A. V. Ustinov, H. Kohlstedt, A. Petraglia, and N. F. Pedersen, Phys. Rev. B **50**, 12 905 (1994).
[11] G. Carapella and G. Costabile, Appl. Phys. Lett. **71**, 3409 (1997).
[12] G. Carapella, G. Costabile, A. Petraglia, N. F. Pedersen, and J. Mygind, Appl. Phys. Lett. **69**, 1300 (1996).
[13] G. Carapella, Phys. Rev. B **59**, 1407 (1999).
[14] S. P. Benz and C. J. Burroughs, Appl. Phys. Lett. **58**, 2162 (1991).
[15] H. S. J. van der Zant, D. Berman, and T. P. Orlando, Phys. Rev. B **49**, 12 945 (1994).
[16] A. V. Ustinov, M. Cirillo, B. H. Larsen, V. A. Obozonov, P. Carelli, and G. Rotoli, Phys. Rev. B **51**, 3081 (1995).
[17] P. Caputo, A. E. Duwell, T. P. Orlando, A. V. Ustinov, N. C. H. Lin, and S. P. Yukon, *Proceedings of ISEC '97*, edited by H. Koch and S. Knappe (Physikalische-Technische Bundesansalt, Braunschweig, 1997).
[18] R. Monaco, S. Pagano, and G. Costabile, Phys. Lett. A **131**, 122 (1988).
[19] G. Carapella, G. Costabile, and P. Sabatino, Phys. Rev. B **58**, 15 094 (1998).
[20] M. A. Itzler and M. Tinkham, Phys. Rev. B **51**, 435 (1995).
[21] G. Carapella, G. Costabile, S. Sakai, and N. F. Pedersen, Phys. Rev. B **58**, 6497 (1998).
[22] S. Pagano, Ph.D. thesis, The Technical University of Denmark, 1987.

[23] N. Grønbech-Jensen, D. Cai, and M. R. Samuelsen, Phys. Rev. B **48**, 16 160 (1993).
[24] D. W. McLaughlin and A. C. Scott, Phys. Rev. A **18**, 1652 (1978).
[25] V. P. Koshelets, S. V. Shitov, L. V. Filippenko, A. M. Baryshev, H. Golstein, T. de Graauw, W. Luinge, H. Shaeffer, and H. van de Stadt, Appl. Phys. Lett. **68**, 1273 (1996).